International Journal of Thermal Sciences 105 (2016) 218–223

Contents lists available at ScienceDirect

International Journal of Thermal Sciences

journal homepage: www.elsevier.com/locate/ijts

A new archive of heat transfer coefficients from square and chamfered cylinders at angles of attack in crossflow

J.C.K. Tong [a], E.M. Sparrow [b], W.J. Minkowycz [c], J.P. Abraham [d, *]

[a] Arup, Level 5 Festival Walk, 80 Tat Chee Avenue, Kowloon Tong, Kowloon, Hong Kong
[b] University of Minnesota, Department of Mechanical Engineering, 111Church St. SE, Minneapolis, MN 55455, USA
[c] University of Illinois, Chicago, Department of Mechanical and Industrial Engineering, 2039 Engineering Research Facility, 842W. Taylor St., Chicago, IL 60607, USA
[d] University of St. Thomas, School of Engineering, 2115 Summit Ave, St. Paul, MN 55105-1079, USA

ARTICLE INFO

Article history:
Received 27 January 2016
Received in revised form
29 February 2016
Accepted 12 March 2016
Available online 21 March 2016

Keywords:
Forced convection
Nusselt number
Cylinders
Chamfered cylinders
Angle of attack

ABSTRACT

Calculations of convection heat transfer coefficients between a fluid in crossflow and two-dimensional square-cylindrical objects have been performed using numerical simulation. Some calculations included geometries with chamfered corners while others were sharp-edged. The numerical model allows a systematic study of various angles of attack and lengths of chamfer so that the entire range of angles and chamfers were investigated. It was found that the present results are in good agreement with previously published archival values for similar geometries and Reynolds numbers. In this regard, the present work significantly expands the upper bound of the Nusselt–Reynolds correlation.

Comparison among the many investigated geometrical configurations reveals that more extensive chamfering results in a lowered dependence of the Nusselt number on the Reynolds number. In the lower range of the Reynolds numbers dealt with in this study, there was near parity in the Nusselt number values for square and octagonal chamfered cylinders; however, at the higher Reynolds number range (approximately 2,000,000), the octagon Nusselt numbers were ~80% of those of the square for a zero-degree angle of attack. The largest angle of attack (45°) also exhibited Nusselt number values that were comparable for the square and octagonal shapes in the lower range of Reynolds numbers. However, at the higher Reynolds numbers, the results differed by approximately a factor of two (square cylinder Nusselt number is larger than the octagonal Nusselt number). The results calculated here for air are extended to other fluids by a simple calculation involving the ratio of Prandtl numbers.

1. Introduction

The determination of convective heat transfer from blunt objects positioned within a crossflow is simultaneously a classic problem which has been studied for many decades and a problem of current and intense interest. There are many situations in both industrial and academic settings where blunt-object convective heat transfer must be known. Traditionally, information has been based on seminal experimental studies [1,2] which for decades formed the basis for textbook recommendations. Subsequently, many other studies [3–19] have expanded upon these original works by considering other shapes and fluids. The literature was summarized by [20] which recommended Nusselt–Reynolds correlations and also corrected a typographical error which had persisted in the literature for some time.

Since the publication of [20], the field has remained remarkably active with both experimental and numerical simulations of both academic and applied foci [21–44] which largely dealt with heat transfer. While this collection of studies is not necessarily exhaustive, it does encompass numerical simulation, steady and unsteady flow, laminar and turbulent regimes, two- and three-dimensional, confined and unconfined situations.

The numerical model to be used here is the same as that of [45]; however, in that study, only fluid mechanics was investigated. Here, heat transfer is the focus. The results from [45] were compared with a wealth of prior studies that used both numerical and experimental methods [46–60] and were found to be in excellent agreement with respect to hydrodynamic forces, flow patterns, and

* Corresponding author.
E-mail addresses: jimmy.tong@arup.com (J.C.K. Tong), jpabraham@stthomas.edu (J.P. Abraham).

http://dx.doi.org/10.1016/j.ijthermalsci.2016.03.008

timewise fluctuations in the wake region. The excellent agreement establishes confidence in the veracity of the method.

To the authors' best knowledge, there are no published studies which systematically vary the angle of attack of two-dimensional square and chamfered cylinders over the full range of angles of attack for high Reynolds numbers. Additionally, the investigated chamfers spanned all the potential lengths so that square-to-octagonal structures are included. The intention is to provide an archival database of Nusselt–Reynolds correlations for these shapes. Finally, the results will be compared with the currently up-to-date experimentally based correlations.

2. Computational model

The numerical simulation is two-dimensional as shown in Fig. 1 with a width transverse to the figure of 0.5D. The fluid flow direction is shown in the image, and the cylinder is placed centrally in the vertical direction. The cylinder is situated closer to the inlet so that sufficient distance is allowed downstream to capture recirculation and wake phenomena. Beneath the main part of the figure is a callout which illustrates the angle of attack for rotated cylinders.

While the cylinder shown in Fig. 1 is square cornered, other shapes are also studied. Chamfers are added to the square of varying lengths until the square shape becomes octagonal. The definition of the chamfer dimension is shown in Fig. 2. Four values of the CHF were used, 0, 0.05D, 0.1D, and 0.293D.

The cylinder shown in Fig. 1 has a zero degree angle of attack. The angle is defined by the normal vector to the leftmost surface of the cylinder and the direction of the flow. Angles from 0 to 45° were used because the results are repetitive thereafter.

At the inlet, the conditions are steady and uniform velocity. Symmetry conditions (zero gradient on all transported quantities) are enforced on the front and rear surfaces (in the direction normal to Figs. 1 and 2). At the top and bottom surfaces, symmetry is also enforced to represent a series of repeating cylinders so that it is a linear array. The results to be displayed here are not sensitive to this symmetry enforcement however because the upper and lower boundaries of the solution domain are sufficiently far away (as confirmed by numerical simulations using alternative boundary conditions at the top and bottom). At the outlet, weak conditions are unforced (zero second derivative on transported variables), and the mean pressure is prescribed. At the cylinder–fluid interface, no-slip conditions were given.

While the inlet conditions are steady, the flow patterns are inevitably unsteady and consequently a transient solution was obtained. The governing differential equations are based a derivative of the $k-\omega$ methodology of Wilcox [61,62] which are solved on

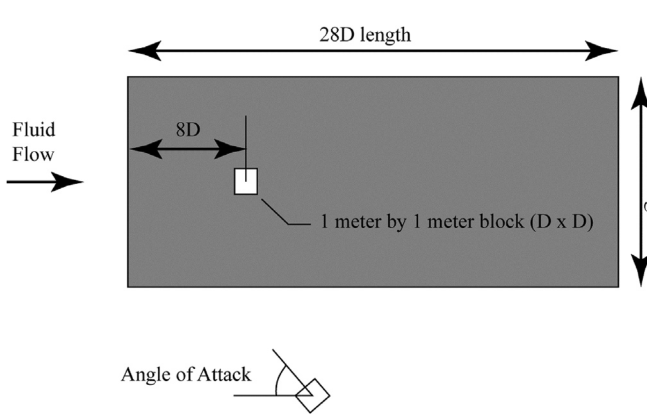

Fig. 1. The solution domain and the angle of attack.

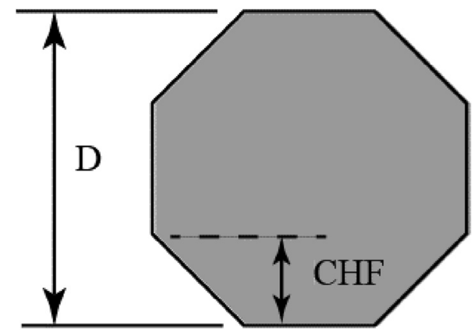

Fig. 2. Definition of the chamfer dimension.

a non-staggered collocated grid using the methods of [63] and [64]. The derivative of this turbulence model is termed the Shear Stress Transport method and is based on the work of Menter [65]. The equations are:

$$\frac{\partial u_i}{\partial x_i} = 0 \tag{1}$$

for conservation of mass and

$$\rho\frac{\partial u_j}{\partial t} + \rho\left(u_i\frac{\partial u_j}{\partial x_i}\right) = -\frac{\partial p}{\partial x_j} + \frac{\partial}{\partial x_i}\left((\mu+\mu_t)\frac{\partial u_j}{\partial x_i}\right) \quad i,j = 1,2,3 \tag{2}$$

for momentum conservation. The quantities μ and μ_t from Eq. (2) are the molecular and turbulent viscosities, respectively.

In addition to conservation of mass and momentum, transport equations for turbulent quantities must be solved. The shear stress transport methodology requires the solution of the turbulent kinetic energy k (Equation (3)) and the specific turbulent intensity ω (Equation (4)).

$$\frac{\partial(\rho k)}{\partial t} + \frac{\partial(\rho u_i k)}{\partial x_i} = P_k - \beta_1\rho k\omega + \frac{\partial}{\partial x_i}\left[\left(\mu + \frac{\mu_t}{\sigma_k}\right)\frac{\partial k}{\partial x_i}\right] \tag{3}$$

and

$$\frac{\partial(\rho\omega)}{\partial t} + \frac{\partial(\rho u_i\omega)}{\partial x_i} = \alpha\rho S^2 - \beta_2\rho\omega^2 + \frac{\partial}{\partial x_i}\left[\left(\mu + \frac{\mu_t}{\sigma_{\omega 1}}\right)\frac{\partial\omega}{\partial x_i}\right] + 2(1-F_1)\rho\frac{1}{\sigma_{\omega 2}\omega}\frac{\partial k}{\partial x_i}\frac{\partial\omega}{\partial x_i} \tag{4}$$

The $k-\omega$ method articulated in [61,62] has a successful record of application to cases such as that investigated here, particularly cases where flow separation occurs. An example of prior applications of this method and extensions to include laminar–turbulent transition are provided in [66–75] and interested readers are directed there.

With the fluid mechanics completely defined, attention is turned to the thermal situation. The energy transport equation is provided in Equation (5).

$$\rho c_p\left(\frac{\partial T}{\partial t}\right) + \rho c_p\left(u_i\frac{\partial T}{\partial x_i}\right) = \frac{\partial}{\partial x_i}\left(k_{eff}\frac{\partial T}{\partial x_i}\right) \tag{5}$$

The effective thermal conductivity k_{eff} represents contributions from the molecular and turbulent conductivities. The turbulent thermal conductivity is quantified by means of the turbulent Prandtl number as in Equation (6)

$$\mathrm{Pr}_{turb} = \frac{c_p\mu_{turb}}{k_{turb}} \tag{6}$$